Enhanced Electric Dipole Strength for the Weakly Bound States in ^{27}Ne

C. Loelius, N. Kobayashi, H. Iwasaki, D. Bazin, J. Belarge, P. C. Bender, B. A. Brown, R. Elder, B. Elman, A. Gade, M. Grinder, S. Heil, A. Hufnagel, B. Longfellow, E. Lunderberg, M. Mathy, T. Otsuka, M. Petri, I. Syndikus, N. Tsunoda, D. Weisshaar, and K. Whitmore

Phys. Rev. Lett. **121**, 262501 — Published 28 December 2018

DOI: 10.1103/PhysRevLett.121.262501

Enhanced electric dipole strength for the weakly bound states in ^{27}Ne

C. Loelius,[1,2] N. Kobayashi,[1,*] H. Iwasaki,[1,2,†] D. Bazin,[1] J. Belarge,[1] P. C. Bender,[1,‡] B. A. Brown,[1,2] R. Elder,[1,2] B. Elman,[1,2] A. Gade,[1,2] M. Grinder,[1,2] S. Heil,[3] A. Hufnagel,[3] B. Longfellow,[1,2] E. Lunderberg,[1,2] M. Mathy,[3] T. Otsuka,[1,4,5,6] M. Petri,[3,7] I. Syndikus,[3] N. Tsunoda,[4] D. Weisshaar,[1] and K. Whitmore[1,2]

[1]*National Superconducting Cyclotron Laboratory, Michigan State University, East Lansing, Michigan 48824, USA*
[2]*Department of Physics and Astronomy, Michigan State University, East Lansing, Michigan 48824, USA*
[3]*Institut für Kernphysik, Technische Universität Darmstadt, Darmstadt, D64289, Germany*
[4]*Center for Nuclear Study, University of Tokyo, 7-3-1 Hongo, Bunkyo-ku, Tokyo, Japan*
[5]*Department of Physics, University of Tokyo, 7-3-1 Hongo, Bunkyo-ku, Tokyo, Japan*
[6]*RIKEN Nishina Center, Wako, Saitama 351-0198, Japan*
[7]*Department of Physics, University of York, Heslington, York YO10 5DD, United Kingdom*

(Dated: November 7, 2018)

An enhanced low-energy electric dipole (E1) strength is identified for the weakly-bound excited states of the neutron-rich isotope ^{27}Ne. The Doppler-shift lifetime measurements employing a combination of the γ-ray tracking array GRETINA, the plunger device, and the S800 spectrograph determine the lower limit of 0.030 e^{2}fm^2 or 0.052 W.u. for the $1/2^+ \rightarrow 3/2^-$ E1 transition in ^{27}Ne, representing one of the strongest E1 strengths observed among the bound discrete states in this mass region. This value is at least 30 times larger than that measured for the $3/2^-$ decay to the $3/2^+_{gs}$ ground state. A comparison of the present results to large-scale shell model calculations points to an important role of core excitations and deformation in the observed E1 enhancement, suggesting a novel example of the electric dipole modes manifested in weakly-bound deformed systems.

Nuclei lying far from stability can demonstrate unique static and dynamic properties due to the extremely asymmetric proton-to-neutron ratios as well as the proximity to the particle-decay threshold. Nuclear halos, which are accompanied by the enhanced low-energy electric dipole (E1) strength, are an example that highlights the unusual structure ascribed to the spatially extended wave function of valence nucleons [1–3]. In light p-shell and psd-shell nuclei close to the neutron drip line, the significant $2s_{1/2}$-wave strength in the ground-state wave function has been recognized to be crucial in halo formation. The resultant strong E1 transitions among associated discrete states have also been observed and interpreted in terms of the excitation of the valence nucleon weakly coupled to a core state [4]. In general, the strong low-energy E1 mode requires two conditions: (1) the shell structure is modified such that a non-normal parity state can intrude at the low excitation energy, and (2) the valence neutron has a small separation energy ($S_n \lesssim 1$ MeV) and occupies a state with the low angular momentum ($\ell = 0,1$), allowing the extended wave function to amplify the E1 strength. Therefore, an observation of enhanced low-energy E1 strengths provides clear evidence for the structural change near the drip line. For an unexplored heavier-mass neutron-rich region, the above picture of the low-energy E1 mode can be altered due to increasing degrees of collectivity and correlations, however, data are still scarce hampering our understanding.

This Letter reports the experimental investigation of the transition strengths among three bound states in the neutron-rich nucleus ^{27}Ne. Lying near the boundary between the sd and pf shells, ^{27}Ne offers new opportunities to study a possible low-energy E1 enhancement in a heavier mass system. The ground state of ^{27}Ne has the spin and parity J^π of $3/2^+_{gs}$ and a relatively low separation energy of $S_n = 1.51$ MeV [5]. Two bound excited states exist at 765(1) keV and 885(2) keV lying below the threshold. The knockout and transfer reaction studies [6–8] have suggested $J^\pi = 3/2^-$ for the 765-keV state and $J^\pi = 1/2^+$ for the 885-keV state, respectively. In a naïve shell model picture, the dominant configurations of the valence neutrons in ^{27}Ne can be assigned as $1d_{3/2}$ for the ground state, $2p_{3/2}$ for the 765-keV state, and $2s_{1/2}$ for the 885-keV state, respectively, indicating both the $3/2^- \rightarrow 3/2^+_{gs}$ and $1/2^+ \rightarrow 3/2^-$ decays to proceed via E1 transitions. Of particular importance is the $1/2^+$ state with the small separation energy of $S_n \approx 0.6$ MeV, since the s-wave character of this weakly-bound state may result in a strong E1 transition, whereas, as discussed later, the state has the $2s^{-1}_{1/2}$ hole configuration and therefore it requires core excitations to induce the E1 enhancement. This makes a sharp contrast to the famous example of ^{11}Be where the $1/2^+$ ground state has a similarly small S_n of ≈ 0.5 MeV but is dominated by the $2s_{1/2}$ particle configuration coupled to the $^{10}\mathrm{Be}_{gs}$ core. The $1/2^- \rightarrow 1/2^+_{gs}$ transition of ^{11}Be displays the very strong E1 strength of 0.11(1) e^{2}fm^2 or 0.36(3) W.u. which has been attributed predominantly to the weakly-bound nature of the states [4].

Additionally, the even-odd ^{27}Ne isotope presents an important testing ground for investigating a possible interplay between the deformation and weakly-bound nature, since the neighboring ^{26,28}Ne isotopes exhibit fairly large quadrupole deformation with $\beta_2 = 0.3-0.4$ [9–11]. Theoretically, it has been shown that the low-ℓ components ($\ell = 0,1$) in the deformed single-neutron orbits be-

come dominant at the limit of weak binding [12, 13], suggesting synergetic effects between collectivity and halo structure. In fact, the recent measurements on the Coulomb and nuclear breakup reactions of the neutron-rich ^{31}Ne and ^{37}Mg isotopes [14, 15] have demonstrated the prevalence of the l=1 components in their ground states, suggesting the formation of a p-wave deformed halo. In the present work, the electric dipole strength among the discrete bound states of ^{27}Ne is investigated, which allows for comparisons with the shell model calculations [16, 17] and therefore provides new insights into the valence-neutron configurations responsible for the E1 enhancement. As a unique experimental approach to determine the E1 strengths in ^{27}Ne, a combined measurement of the branching ratio and lifetimes of the excited states was performed at the National Superconducting Cyclotron Laboratory (NSCL).

A primary beam of ^{48}Ca was accelerated up to 140 MeV/nucleon at the NSCL Coupled Cyclotron Facility and impinged on a Be production target. A secondary beam of ^{29}Na at 90.5 MeV/nucleon was produced and separated by the A1900 fragment separator [18]. The ^{9}Be(^{29}Na,^{27}Ne) reaction was used to populate the excited states of interest and the S800 spectrograph [19] was used to identify reaction products. First, a measurement was performed only with a 1.0-mm-thick ^{9}Be target to determine the branching ratio of the $1/2^+$ decay. Subsequently, the lifetime measurements were performed based on the recoil-distance method [20] using a combination of the 1.0-mm-thick ^{9}Be target and 0.92-mm-thick Ta degrader separated at a near-contact 50-μm distance. This resulted in two different recoil velocities ($\beta = v/c$) before and after the Ta degrader which are denoted as fast ($\beta_{\rm fast} = 0.40$) and slow ($\beta_{\rm slow} = 0.34$), respectively. Data were also taken with a large-distance (25-mm) setting to evaluate backgrounds due to reactions occurring in the degrader.

Nine GRETINA detectors [21, 22] consisting of 36 high-purity germanium crystals were used to measure the energies and hit positions of emitted γ rays in coincidence with reaction products. The TRIPLEX plunger device [23] was mounted about 13 cm upstream of the center of GRETINA to facilitate the recoil-distance measurements [24–26]. Four detectors covered the forward-most angles between 20 and 50 degrees, whereas the remaining five detectors were positioned at angles around 70 degrees. For the lifetime measurements, the events are selected for the laboratory angles below 40 degrees to ensure the sensitivity to the Doppler shifts. Addback of multiple γ-ray interactions in GRETINA, Doppler-shift correction with the track information of the reaction products, and the evaluation of neutron-induced backgrounds were performed as described in Ref. [25].

The Doppler-corrected γ-ray spectrum of ^{27}Ne measured in the single target setup is shown in Fig.1. Three γ-ray peaks corresponding to the $1/2^+ \rightarrow 3/2^-$ transition at 120 keV, the $3/2^- \rightarrow 3/2^+_{gs}$ transition at 765 keV, and the $1/2^+ \rightarrow 3/2^+_{gs}$ transition at 885 keV are clearly observed with the energy resolution of ≈2% (FWHM) in this measurement. Note that a sizable branch observed for the 120-keV decay originated from the $1/2^+$ state at 885 keV is indicative of a strong E1 strength of the $1/2^+ \rightarrow 3/2^-$ transition, given that the other M1/E2 decay branch has a much larger level spacing of 885 keV. The branching ratios are deduced to be $17 \pm 3\%$ and $83 \pm 3\%$ for the $1/2^+$ decay to the $3/2^-$ and $3/2^+_{gs}$ states, respectively, which agree well with the previous results ($16.2 \pm 2.0\%$ and $83.8 \pm 2.0\%$) [6].

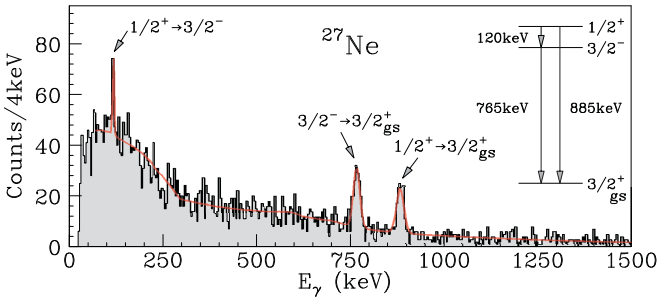

FIG. 1. Doppler-corrected γ-ray spectrum measured in the ^{9}Be(^{29}Na,^{27}Ne) reaction is compared with the simulation including an exponential background. The additional low-energy background is determined based on the quadratic fit to a reference spectrum obtained from the neighboring ^{28}Ne isotope.

Figure 2 shows the Doppler-corrected γ-ray spectra obtained from the recoil-distance lifetime measurements of ^{27}Ne. In Fig. 2 (a), the Doppler-shift correction is optimized for the slow components, but only the fast components are evident for both the decays from the $3/2^-$ and $1/2^+$ states. A clear absence of the slow component for the 885-keV transition suggests a very short lifetime of the state, however, the low-energy tail visible for the 765-keV peak indicates that the lifetime should be in the measurable range based on its spectral shape. Therefore, the lifetimes are studied via the spectral shape analysis employing GEANT4-based simulations [24–27] that incorporate all important aspects of experimental conditions. The neutron-induced background contributions present a peak structure after Doppler-shift correction [25] as only forward-angle data are used for Fig 2 (a). Following the procedure of Ref. [25], the background yields were first constrained using the laboratory-frame spectra and then included in the fit by simulating corresponding spectra for the projectile frame. The χ^2 distributions shown in Fig. 2 (b) are the results obtained from the fits to the 765-keV (Fig. 2 (c)) and 885-keV (Fig. 2 (d)) spectra. The mean lifetime (τ) of the $3/2^-$ state at 765 keV is determined to be 2.1±0.5 ps based on the method [28] by scaling up the statistical uncertainties by the square root of the reduced χ^2 value. The quoted error is the

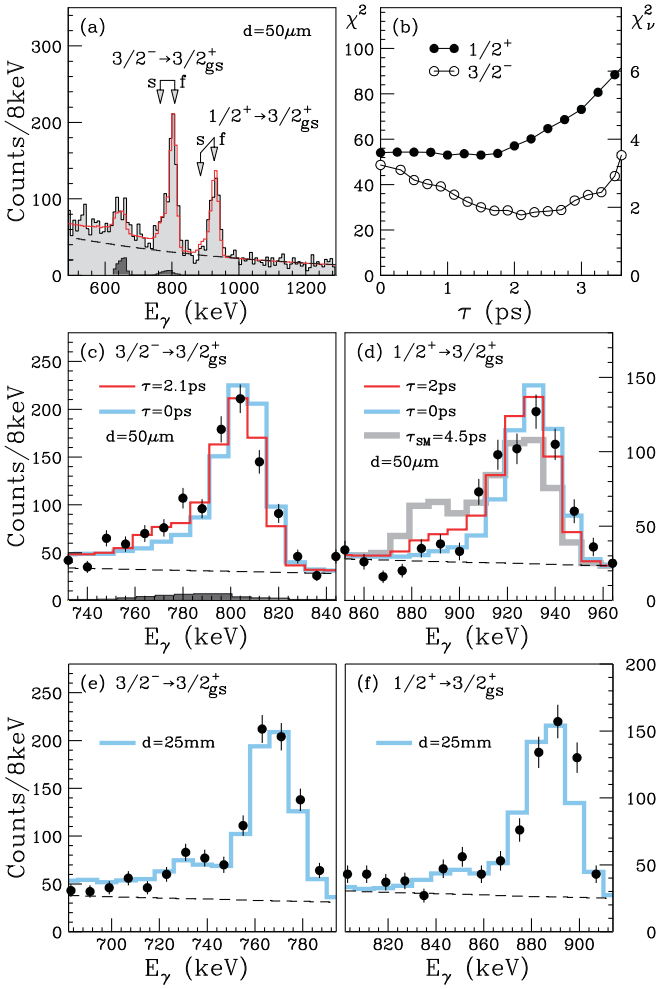

FIG. 2. Doppler-corrected γ-ray spectrum from the recoil-distance lifetime measurements of ^{27}Ne with the d = 50μm distance setting is shown in (a). The arrows indicate the fast (f) and slow (s) components. The backgrond contributions due to reactions of neutrons onto ^{27}Al and ^{72}Ge [25] are shown by the dark histogram. The panel (b) shows the χ^2 distributions (with the reduced χ^2 on the right axis) from the fits to the spectra for the $3/2^-$ decay (c) and the $1/2^+$ decay (d). In (c) and (d), the data are compared to simulated histograms with different lifetimes; the present results (red), the reference value of 0 ps (blue), and the EEdf1 shell-model prediction of 4.5 ps (gray, see text), including background (dashed lines). In the bottom panels, Doppler-corrected γ-ray spectra taken with the large distance setting (d = 25mm) are shown for the $3/2^-$ (e) and $1/2^+$ (f) decays.

quadratic sum of the statistical uncertainty (0.4 ps) and systematic ambiguities (0.3 ps) such as due to the feeding from the $1/2^+$ state and the background from reactions in the degrader. As for the $1/2^+$ state at 885 keV, the minimum χ^2 value is found at τ = 1.5 ps although the χ^2 distribution is rather flat toward 0 ps with a reduced χ^2~3.5. Therefore, an upper limit (1σ) of τ = 2.0 ps is determined for the $1/2^+$ state, where the consideration of the systematic error leaves this upper bound unchanged.

In Figs. 2 (c) and (d), the measured spectra are also compared to the simulated spectra with the lifetime of 0 ps (blue histograms) in addition to the present lifetime results (red histograms for Figs. 2 (a), (c), and (d)). In the comparison for the 765-keV transition (Fig. 2 (c)), the excess of the yield at the slow component is clearly demonstrated, whereas the data for the 885-keV state (Fig. 2 (d)) are consistent with either of the two simulations with τ= 0 and 2 ps, confirming the present conclusions. Since the present results rely on an understanding of the spectral shape in the region of the slow components which could be affected by Compton scattering or low-energy tails of the fast components if they existed, the additional spectra from the 25-mm distance setting are shown in Figs. 2 (e) and (f) as a reference. Note that the neutron-induced backgrounds have only marginal contributions to the region of interest (Fig 2 (c)). In order to gain statistics, all events from GRETINA without the angle gates were used for these spectra and the Doppler-shift correction was optimized for the fast velocity and the target position. In this specific case, fast and slow components are expected to be well separated due to combined effects of over-corrected velocities and under-corrected γ-detection angles used in the Doppler-shift correction for the degrader (slow) components [29]. Since the excited states produced in the target are expected to completely decay before reaching the degrader, the spectra shown in Figs. 2 (e) and (f) are not sensitive to the lifetimes of the states, but provide useful measurements to constrain the reaction contributions from the degrader. The relative degrader contributions are determiend separately for each state and found to be as small as ≈15%. The simulations which take into account the degrader contributions reproduce the measured spectra very well, demonstrating that the reference simulations (blue histograms) shown in Figs. 2 (c) and (d) indeed provide reliable baselines for the lifetime analysis.

The present results of $B(E1; 1/2^+ \rightarrow 3/2^-)$ and $B(E1; 3/2^- \rightarrow 3/2^+_{gs})$ in ^{27}Ne are obtained by combining the measured branching ratios and lifetimes and summarized in Table I. The $B(E1; 1/2^+ \rightarrow 3/2^-)$ is found to have a lower bound of 0.030 e^2fm^2 or 0.052 W.u. from the lifetime of the $1/2^+$ state and the branching ratio of the $1/2^+$ decay to the $3/2^-$ state. The $B(E1; 3/2^- \rightarrow 3/2^+_{gs})$

TABLE I. The E1 transition strengths (e^{2}fm^2) in ^{27}Ne measured in the present work compared to the shell model calculations with the WBP-M and EEdf1 interactions.

^{27}Ne	Exp	WBP-M	EEdf1
$B(E1; 1/2^+ \rightarrow 3/2^-)$	$> 3.0 \times 10^{-2}$	7.5×10^{-3}	1.4×10^{-2}
$B(E1; 3/2^- \rightarrow 3/2^+_{gs})$	$6.7^{+2.1}_{-1.3} \times 10^{-4}$	4.1×10^{-4}	6.7×10^{-3}

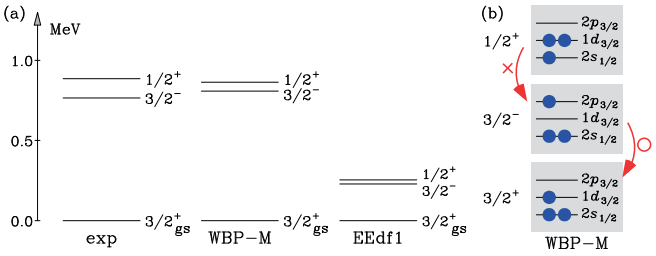

FIG. 3. (a) The level scheme of ^{27}Ne is compared to the WBP-M and EEdf1 shell-model calculations. (b) The dominant configurations given by the WBP-M calculations are illustrated for three valence neutrons outside the fully occupied $1d_{5/2}$ orbital. The diagrams with the arrows indicate the allowed (◯) or forbidden (×) E1 transitions among the states.

is determined by the lifetime of the $3/2^-$ state and is found to be $6.7^{+2.1}_{-1.3} \times 10^{-4}$ e^2fm^2 or $1.2^{+0.3}_{-0.3} \times 10^{-3}$ W.u. It should be noted that the lower limit of the E1 transition rate obtained for the $1/2^+$ decay is at least 30 times stronger than that measured for the $3/2^-$ decay, representing one of the strongest E1 transition strengths observed among the low-lying bound states in *sd*-shell nuclei [5, 30].

In order to understand the valence-neutron configurations responsible for the strong E1 enhancement in ^{27}Ne, large-scale shell model calculations were performed. First, calculations were performed in the $1s-1p-2s1d-1f2p$ shell model space [16] using the WBP Hamiltonian with a modification to reduce the $sd-pf$ gap by 0.7 MeV [8]. The calculations (denoted as WBP-M) were performed by allowing for a maximum of $1\hbar\omega$ ($1p1h$) excitations for both protons and neutrons and therefore the present results for positive-parity states correspond to those from the USD interaction used for the *sd*-part of the WBP Hamiltonian. The present calculations well reproduce the level scheme as shown in Fig. 3 (a).

The E1 transition rates are also calculated using the isovector dipole transition operator $e\frac{Z}{A}\sum_{i=1}^{N} r_i Y_{1\mu}(r_i) - e\frac{N}{A}\sum_{i=1}^{Z} r_i Y_{1\mu}(r_i)$ where the spurious center-of-mass motion is subtracted. The radial integrals are calculated on the harmonic oscillator basis. As shown in Table I, the present calculations agree well with the B(E1) measured for the $3/2^- \rightarrow 3/2^+_{gs}$ transition, but the strength calculated for the $1/2^+$ decay is smaller at least by a factor of 4. As illustrated in Fig. 3 (b), the dominant components for the $3/2^-$ and $3/2^+_{gs}$ states correspond to the intruder $2p_{3/2}$ and normal $1d_{3/2}$ configurations coupled to the lowest configuration of ^{26}Ne, respectively. The E1 transition between these dominant configurations is allowed but the overall strength remains hindered due to the small E1 single-particle transition strength between the $1d_{3/2}$ and $2p_{3/2}$ orbitals and the destructive interference with other strengths. As for the $1/2^+$ state, the single-particle transition strength between the $2s_{1/2}$ and $2p_{3/2}$ orbitals gives dominant contributions, however, the E1 transition between the dominant configurations (Fig. 3 (b)) is forbidden, since the $1/2^+$ state of ^{27}Ne corresponds to the $2s^{-1}_{1/2}$ hole state. Therefore it requires core excitations in either $1/2^+$ or $3/2^-$ state to yield a finite E1 strength. Besides, possible effects due to spatially extended wave function of the $1/2^+$ state cannot be included in the calculations because the $2s^{-1}_{1/2}$ hole state should be regarded as a $2s_{1/2}$ particle state tightly bound to an excited core state of ^{26}Ne, following the common prescription [4]. In fact, the result of B(E1) does not change significantly even if the calculations are performed with the radial wave functions derived from Skyme Hartree-Fock models unless an unphysically small binding energy is assumed for the $2s_{1/2}$ single-particle orbital.

The nuclear region in the vicinity of ^{27}Ne is known as the island of inversion [31] where the neutron $2p2h$ and $4p4h$ configurations across the $N = 20$ shell gap dominate the ground states enhancing quadrupole collectivity. Such intruder configurations may play an important role in the dipole excitation of ^{27}Ne, since the lowest configurations (Fig. 3 (b)) do not allow for the E1 transition between the $1/2^+$ and $3/2^-$ states. Therefore, further shell model calculations were performed (denoted as EEdf1 [17, 32]) in the *sdpf* model space including up to $6p6h$ excitations from the *sd* shell to *pf* shell by applying the recently developed extended Kuo-Krenciglowa (EKK) theory of the effective nucleon-nucleon interaction. The EKK calculation provides a microscopic shell-model description of nuclear properties in the island of inversion without fit of the interaction [17]. The level energies of the EEdf1 calculations differ from data by about 0.5 MeV, but no adjustments are made for the single-particle energies as determined in Ref. [17]. However, the calculated spectroscopic factors for the $d(^{26}\mathrm{Ne},^{27}\mathrm{Ne})p$ reaction are 0.46, 0.44, 0.19 for the $3/2^+$, $3/2^-$, $1/2^+$ states of ^{27}Ne, respectively, showing a good agreement with the data (0.42(22), 0.64(33), 0.17(14) for the $3/2^+$, $3/2^-$, $1/2^+$ states) as well as the WBP-M calculations [8]. A notable difference in the EEdf1 results is the sizable intruder components found for the positive-parity states of ^{27}Ne as well as the ground state of ^{26}Ne. The $3/2^+_{gs}$ state of ^{27}Ne have about 30% $2p2h$ components which are comparable to those obtained for the ground state of ^{26}Ne. These components become more dominant (about 70%) for the $1/2^+$ state in ^{27}Ne, whereas the $3/2^-$ state remains in the normal $1p1h$ configuration (about 80%). The larger values of B(E1) are obtained for both the decays (Table I) due to the increased role of the $1f_{7/2}-1d_{5/2}$ transition, accounting partly for the E1 enhancement. However, the absolute strength for the $1/2^+$ decay and its enhancement relative to the $3/2^-$ decay still remain too small. For comparison, the corresponding spectrum with the theoretical lifetime of $\tau_{\mathrm{SM}} = 4.5$ ps obtained from the EEdf1 calculation and measured branching ra-

tio is shown in Fig. 2 (d).

The strong E1 transition presently identified for ^{27}Ne represents a novel example because the E1 transition is associated with the $2s^{-1}_{1/2}$ hole state in the shell-model picture and therefore it requires core excitations to induce the E1 enhancement unlike other known cases in light nuclei [4]. The present case also provides a challenge for our understanding of dipole excitations in neutron-rich systems, since physics mechanisms involving the modification of the shell structure, the core excitation and deformation, and weakly-bound effects near the threshold [33] would need to be incorporated to fully comprehend the origin of the E1 enhancement. Concerning the collectivity, both the shell model calculations predict fairly large M1 and E2 strengths [34] (WBP-M: B(M1) of 6.0×10^{-2} W.u. and B(E2) of 6.0 W.u., EEdf1: B(M1) of 2.2×10^{-2} W.u. and B(E2) of 6.2 W.u.) for the $1/2^+ \rightarrow 3/2^+_{gs}$ transition. The corresponding theoretical partial lifetime of 0.8−2.0 ps is comparable to the upper limit of 2.4 ps experimentally constrained from the upper bound of the $1/2^+$ lifetime and the branching ratio for the $1/2^+$ decay to the $3/2^+_{gs}$ state. In this respect, it is interesting to note that the configurations of the $3/2^-$ and $1/2^+$ states in ^{27}Ne may correspond to $[Nn_z\lambda\Omega] = [330\ 1/2]$ and $[200\ 1/2]$ Nilsson orbitals at the deformation of $\beta_2 \approx 0.4$ [35], respectively. In this picture, the E1 transition can be viewed as the single-particle excitation of the valence neutron weakly bound to the deformed core [36], suggesting the deformation as an important ingredient to account for the E1 enhancement.

In summary, a strong low-energy E1 transition has been found in the neutron-rich ^{27}Ne isotope from excited-state lifetime measurements with GRETINA. A comparison of this result with large-scale shell model calculations indicates that core excitations and deformation are key mechanisms in inducing the E1 enhancement, emphasizing the importance of further studies to pin down the absolute E1 strength and its origin. The present data provides the first example of strong E1 transitions occurring in the weakly bound states of neutron-rich nuclei in the vicinity of the island of inversion, highlighting the intriguing interplay of the shell erosion, deformation, and weakly-bound nature of nuclei far from stability.

This work was supported by the National Science Foundation (NSF) under PHY-1102511, PHY-1565546 and PHY-1811855, by the Department of Energy (DOE) National Nuclear Security Administration through the Nuclear Science and Security Consortium under Award Numbers DE-NA0000979 and DE-NA0003180, and by the Royal Society under contract number UF150476 and the Deutsche Forschungsgemeinschaft through SFB 1245. GRETINA was funded by the DOE, Office of Science. Operation of the array at NSCL was supported by DOE under Grant No. DE-SC0014537 (NSCL) and DE-AC02-05CH11231 (LBNL). This work was also supported in part by HPCI Strategic Program (hp150224), by MEXT and JICFuS as a priority issue (elucidation of the fundamental laws and evolution of the universe) to be tackled by using Post "K" Computer (hp160211, hp170230), by the HPCI system research project (hp170182), and by the CNS-RIKEN joint project for large-scale nuclear structure calculations.

* Present address: Research Center for Nuclear Physics, Osaka University, Ibaraki, Osaka 567-0047, Japan
† iwasaki@nscl.msu.edu
‡ Present address: Department of Physics, University of Massachusetts Lowell, Lowell, Massachusetts 01854, USA

[1] I. Tanihata, *et al.*, Phys. Rev. Lett. 55, 2676 (1985).
[2] P. G. Hansen and B. Johnson, Europhys. Lett. 4, 409 (1987).
[3] T. Aumann and T. Nakamura, Phys. Scr. T152, 014012 (2013).
[4] D. J. Millener, J. W. Olness, E. K. Warburton, and S. S. Hanna, Phys. Rev. C **28**, 497 (1983).
[5] Evaluated Nuclear Structure Data File (ENSDF), http://www.nndc.bnl.gov/ensdf.
[6] J. R. Terry *et al.*, Phys. Lett. B **640**, 86 (2006).
[7] A. Obertelli, *et al.*, Phys. Lett. B **633**, 33 (2006).
[8] S. M. Brown, *et al.*, Phys. Rev. C **85**, 011302(R) (2012).
[9] B. Pritychenko *et al.*, Phys. Lett. B **461**, 322 (1999).
[10] H. Iwasaki, *et al.*, Phys. Lett. B **620**, 118 (2005).
[11] J. Gibelin, *et al.*, Phys. Rev. C **75**, 057306 (2007).
[12] Ikuko Hamamoto, Phys. Rev. C **69**, 041306(R) (2004).
[13] T. Misu, W. Nazarewicz, and S. Averg, Nucl. Phys. A **614**, 44 (1997).
[14] T. Nakamura, *et al.*, Phys. Rev. Lett. **112**, 142501 (2014).
[15] N. Kobayashi, *et al.*, Phys. Rev. Lett **112**, 242501 (2014).
[16] E. K. Warburton and B. A. Brown, Phys. Rev. C **46**, 923 (1992).
[17] N. Tsunoda, *et al.*, Phys. Rev. C **95**, 021304(R) (2017).
[18] D. J. Morrissey *et al.*, Nucl. Instrum. Meth. B **204**, 90 (2003).
[19] D. Bazin *et al.*, Nucl. Instrum. Meth. B **204**, 629 (2003).
[20] A. Dewald, *et al.*, Prog. Part. Nucl. Phys. **67**, 786 (2012).
[21] S. Paschalis *et al.*, Nucl. Instrum. Meth. A **709**, 44 (2013).
[22] D. Weisshaar *et al.*, Nucl. Instrum. Meth. A **847**, 187 (2017).
[23] H. Iwasaki, *et al.*, Nucl. Instrum. Meth. A **806**, 123 (2016).
[24] H. Iwasaki, *et al.*, Phys. Rev. Lett. **112**, 142502 (2014).
[25] C. Loelius, *et al.*, Phys. Rev. C **94**, 024340 (2016).
[26] T. Mijatovic', *et al.*, Phys. Rev. Lett. **121**, 012501 (2018).
[27] P. Adrich *et al.*, Nucl. Instrum. Meth. A **598**, 454 (2009).
[28] C.Patrignani, P.D.Group, Chin. Phys. C40, 100001 (2016).
[29] C. Loelius, Ph.D thesis (2017), Michiga State University, *unpublished.*
[30] P. M. Endt, Atomic Data and Nucl. Data Tables **23**, 3 (1979).
[31] E. K. Warburton, J. A. Becker, and B. A. Brown, Phys. Rev. C **41**, 1147 (1990).
[32] B. Fernández-Domínguez, *et al.*, Phys. Lett. B **779**, 124 (2018).
[33] K. Fossez, J. Rotureau, N. Michel, Quan Liu, and

W. Nazarewicz, Phys. Rev. C **94**, 054302 (2016).
[34] W. A. Richter, S. Mkhize, B. A. Brown, Phys. Rev. C **78**, 064302 (2008).
[35] N. Kobayashi, *et al.*, Phys. Rev. C **93**, 014613 (2016).
[36] I. Hamamoto and S. Shimoura, J. Phys. G: Nucl. Part. Phys. **34**, 2715 (2007).